

Review Article

Open Access

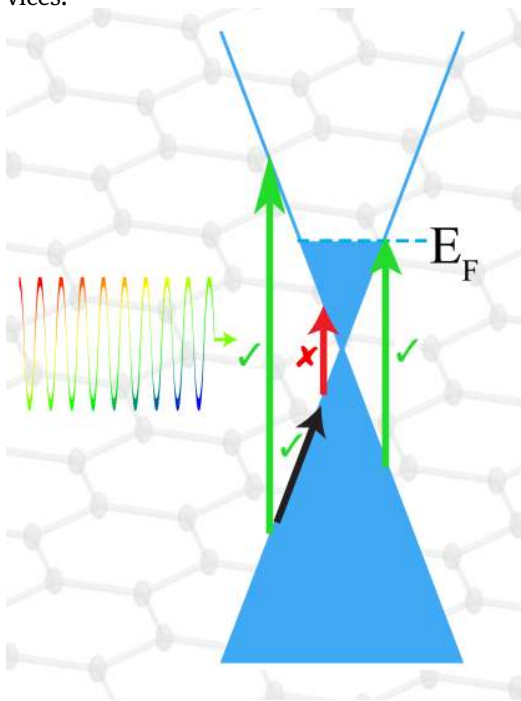
Naresh Kumar Emani, Alexander V. Kildishev, Vladimir M. Shalaev, and Alexandra Boltasseva*

Graphene: A Dynamic Platform for Electrical Control of Plasmonic Resonance

DOI 10.1515/nanoph-2015-0014

Received October 30, 2014; accepted May 25, 2015

Abstract: Graphene has recently emerged as a viable platform for integrated optoelectronic and hybrid photonic devices because of its unique properties. The optical properties of graphene can be dynamically controlled by electrical voltage and have been used to modulate the plasmons in noble metal nanostructures. Graphene has also been shown to support highly confined intrinsic plasmons, with properties that can be tuned in the wavelength range of 2 μm to 100 μm . Here we review the recent development in graphene-plasmonic devices and identify some of the key challenges for practical applications of such hybrid devices.



Keywords: Electrical control; plasmon resonance; graphene plasmonics; numerical modeling; IR modulators

*Corresponding Author: **Alexandra Boltasseva:** School of Electrical and Computer Engineering and Birck Nanotechnology Center, Purdue University, West Lafayette, IN 47907, USA


1 Introduction

Nanophotonics is a thriving research field, which holds tremendous promise for optical information processing at the nanoscale. One of the most promising directions in nanophotonics is to use free charge oscillations in metal nanostructures known as surface plasmons (SPs) for control and manipulation of optical signals [1, 2]. Surface plasmons exhibit a resonant behavior at a particular wavelength, when the electric restoring force equals the Lorentz force caused by an incident field. At such a resonance the electromagnetic energy is confined to subwavelength length scales in the close vicinity of the nanostructures. This unprecedented ability to confine energy in small volumes has resulted in a number of novel applications like surface plasmon assisted lithography [3], data storage [4], enhanced chemical reaction rates [5, 6], improved photovoltaic devices [7], particle trapping [8, 9], and biosensing [10].

At present, there are two main challenges in realizing the full promise of plasmonics. First, the traditional noble metals (gold and silver) used in plasmonics exhibit relatively high intrinsic optical loss. They are also not fully CMOS compatible and hence cannot be integrated with electronic components. In recent years a number of significant breakthroughs were made in identifying alternative plasmonic materials [11]. Naik et al. demonstrated that transparent conducting oxides like aluminum doped zinc oxide, and ceramic nitrides like TiN can be used to lower losses and thereby improve the performance of plasmonic devices [12, 13]. The second major challenge in plasmonics is the lack of post fabrication dynamic control of plasmonic resonance. Currently the resonant wavelength of plasmonic nanostructures is dependent on their

and DTU Fotonik, Department of Photonics Engineering, Technical University of Denmark, Lyngby, DK-2800, Denmark, E-mail: aeb@purdue.edu

Naresh Kumar Emani, Alexander V. Kildishev, Vladimir M. Shalaev: School of Electrical and Computer Engineering and Birck Nanotechnology Center, Purdue University, West Lafayette, IN 47907, USA

 © 2015 Naresh Kumar Emani *et al.*, licensee De Gruyter Open. This work is licensed under the Creative Commons Attribution-NonCommercial-NoDerivs 3.0 License.

size, shape, and material properties [1, 14]. In the literature we find that a number of phenomena like phase transitions [15], electrical carrier injection in semiconductors [16, 17], ultrafast optical pumping [18] and mechanical stretching of elastic membranes [19, 20] have been used to tune plasmonic resonances. The magnitude and speed of change in resonance are important criteria in evaluating the merits of these approaches for specific applications.

Recently the synergy between the exceptional optoelectrical properties of graphene and plasmon resonances in metallic nanostructures led to the development of electrically modulated plasmonic resonance. These devices can potentially lead to applications like modulators, photodetectors, and sensors in near-infrared (NIR) to mid-infrared (MIR) wavelength ranges. In this review we begin with a discussion of the fundamental optical properties of graphene, which makes it very attractive for the dynamic control of plasmon resonance. We also describe numerical approaches to model graphene using full wave electromagnetic simulations. We then survey the current status of graphene-hybrid devices in MIR and NIR wavelength ranges. We then identify current difficulties, and present our perspective of this exciting new research direction.

2 Optical properties of graphene

2.1 Band structure of graphene

Graphene is a hexagonal lattice of sp^2 hybridized carbon atoms arranged in a single atomic layer. In the crystalline phase, the electronic configuration of carbon is $1s^2$, $2s^2$, $2p^2$. The $2s$ and $2p$ orbitals can mix with each other in three possible ways giving rise to sp , sp^2 , and sp^3 hybridizations forming different carbon-based molecules [21]. In the reciprocal space, the unit cell can be described by two basis vectors \vec{a}_1 and \vec{a}_2 as shown in Fig. 1. Starting from these basis vectors and using the tight binding approximation [21] it can be shown that the band structure can be described using the equation

$$E(\vec{k}) = \pm \gamma_0 \sqrt{1 + 4 \cos \frac{\sqrt{3}k_x a_0}{2} \cos \frac{k_y a_0}{2} + 4 \cos^2 \frac{k_y a_0}{2}} \quad (1)$$

where, a_0 is the lattice constant, k_x and k_y are reciprocal lattice vectors, and γ_0 is the nearest neighbor hopping energy (typically in the range 2.6–3.1 eV).

The conduction and valance bands touch each other at the six corners of the hexagonal 1st Brillouin zone known as the K points as shown in Fig. 1b. Close to the K points the dispersion relation for graphene is linear ($E = \hbar v_F k$).

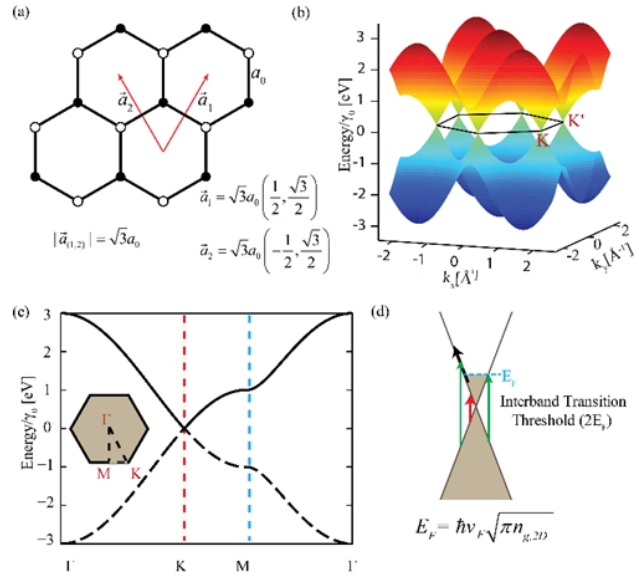


Figure 1: Electronic band structure of graphene: (a) Unit cell in reciprocal space showing the basis vectors \vec{a}_1 and \vec{a}_2 in terms of real space lattice constant a_0 . (b) The E-K diagram for graphene (eq. 1) calculated using the tight binding approximation. The conduction and valance bands meet at the six corners of the hexagon in reciprocal space (known as Dirac or K points). The energy scale is normalized to nearest-neighbor hopping energy which is typically in the range 2.6–3.1 eV. (c) Simplified representation of band structure of graphene using cut-lines along high symmetry directions. The band structure is linear close to K points giving rise to many unique properties of graphene. (d) Intra-band and inter-band transitions in graphene, photons with energies above $2E_F$ will be absorbed due to transitions into the unoccupied states above the Fermi level.

The Fermi energy (E_F) is given by

$$E_F = \hbar v_F k_F = \hbar v_F \sqrt{\pi n_{g,2D}} \quad (2)$$

where, $n_{g,2D}$ is the carrier concentration in the two-dimensional graphene sheet, v_F is the Fermi velocity ($\approx 1 \times 10^6$ m/s). This linear dispersion implies that charge carriers in graphene behave as massless Dirac fermions. This is the underlying reason for many novel electronic and optical properties of graphene like large carrier mobility (and hence low DC scattering rate) and allowed inter-band transitions from terahertz to visible frequencies [22, 23]. It can easily be shown that this linear dispersion results in a linear dependence of the electronic density of states (DOS) on the Fermi wavevector (k_F) around Dirac point which is given by

$$DOS(k_F) = \frac{k_F}{\pi \hbar v_F} = \frac{\omega}{\pi \hbar v_F^2} \quad (3)$$

Therefore, undoped graphene is extremely sensitive to small external perturbation especially at IR frequencies. This also leads to highly nonlinear current change close to

the Dirac point [24]. This is clearly different from a conventional 2D electron gas, with parabolic dispersion, where the density of states is constant ($m^*/\pi\hbar^2$). Further, the sheet carrier density can be electrically tuned by electrostatic gating using a field effect transistor (FET) structure. Due to these fascinating electrical properties, graphene was initially considered as an alternative to silicon for nanoelectronics.

2.2 Intraband and interband transitions in graphene

The electronic properties and optical properties of graphene are very closely related. In undoped graphene at 0 K, optical absorption is frequency independent—determined only by universal absorbance, $A(\omega) = \pi e^2/\hbar c = \pi\alpha \approx 2.3\%$ [23]. This is due to the cancellation of frequency dependent terms in the three important parameters determining optical absorption in Fermi golden rule—the square of transition matrix element ($\propto v_F^2/\omega^2$), the joint density of states ($\propto \omega/\hbar v_F^2$), and the photon energy ($\propto \omega$) [25].

The optical absorption in doped graphene depends strongly on the sheet carrier density. A photon incident on a graphene sheet can excite two types of possible transitions—an intraband transition where the initial and final states of the electron are within the same band, and an interband transition where the incident photon excites an electron in valance band into the conduction band (see Fig. 1d). Further, an interband transition can generate an e-h pair only if the energy of the incident photon is greater than $2E_F$. These transitions can be analytically expressed in terms of optical conductivity of graphene derived under the Random Phase Approximation (RPA) in the local limit as [26–28]:

$$\sigma(\omega) = \frac{2e^2\omega_T}{\pi\hbar} \frac{i}{\omega + i\tau^{-1}} \log \left[2 \cosh \left(\frac{\omega_F}{2\omega_T} \right) \right] + \frac{e^2}{4\hbar} \left[H \left(\frac{\omega}{2} \right) + i \frac{2\omega}{\pi} \int_0^\infty \frac{H \left(\frac{\omega'}{2} \right) - H \left(\frac{\omega}{2} \right)}{\omega^2 - \omega'^2} d\omega' \right] \quad (4)$$

where, $H(\omega) = \sinh(\omega/\omega_T)/[\cosh(\omega_F/\omega_T) + \cosh(\omega/\omega_T)]$, $\omega_F = E_F/\hbar$, $\omega_T = k_B T/\hbar$, ω is the frequency of incident light, e is the charge of an electron, τ is the Drude relaxation rate, T is the temperature, and k_B is the Boltzmann constant. The first term represents the free carrier response of graphene arising due to the intraband transitions. The intraband response is dominant above MIR wavelengths as can be seen in Fig. 2(a–b). The second

term describes the contribution of interband transitions, which are the dominant contribution at visible and NIR wavelengths, where the conductance has a constant value of $G_0 (= e^2/4\hbar)$. The optical conductivity calculated using RPA is consistent with numerous experimental reports in literature [23, 29, 30].

2.3 Numerical Modeling of Graphene

To develop useful devices with graphene it is essential to develop accurate models for numerical simulations. Graphene being a vanishingly thin monolayer poses unique challenges for numerical treatment. There are two main approaches for the numerical implementation of graphene (i) treat graphene as an effective medium with finite thickness (t_g) [31] and permittivity given by $\epsilon(\omega) = 1 + i\sigma(\omega)/\omega\epsilon_0 t_g$, (ii) describe graphene with a surface current $J_s = \sigma(\omega)E$. In the first approach there can be stability and convergence problems if the choice of t_g is not sufficiently small. Further, an extremely small thickness will add unnecessary computational complexity due to the requirement of a fine mesh size [32]. Hence, the second approach is more suited for grid-based, full-wave finite-element frequency domain simulation methods using for example commercial tools such as COMSOL Multiphysics or CST Studio. The validity of the numerical modeling can be seen in Fig. 3 where the experimentally measured IR reflectivity of single layer graphene (SLG) normalized to reflectivity at charge neutral point (CNP) is shown along with the numerical simulations. When the carrier density is increased SLG becomes more “metallic” and hence reflectivity is higher. The dip seen in the 9–10 μm range is due to the optical phonon in the SiO_2 layer which leads a large reflection peak and an effectively small change as a function of carrier density. The features at 8 μm are related to the epsilon near zero enhanced absorption which appear when reflection from a range of angle of incidence (ϕ) is measured. We can see from Fig. 3(b) that simulation at normal incidence alone does not capture the experimental data. To better match the experimental features we averaged simulations over a range of ϕ —the full details of which are discussed in an upcoming paper. The final result of the averaging procedure is shown in Fig. 3(c) which indicates the RPA model is able to capture the behavior of graphene remarkably well considering that the experiments were performed using Chemical Vapor Deposition (CVD) grown with up to 20% inhomogeneity. An important point to note is that the scattering time extracted from our experimental and numerical analysis is about five times smaller than estimate based on DC Drude model [33].

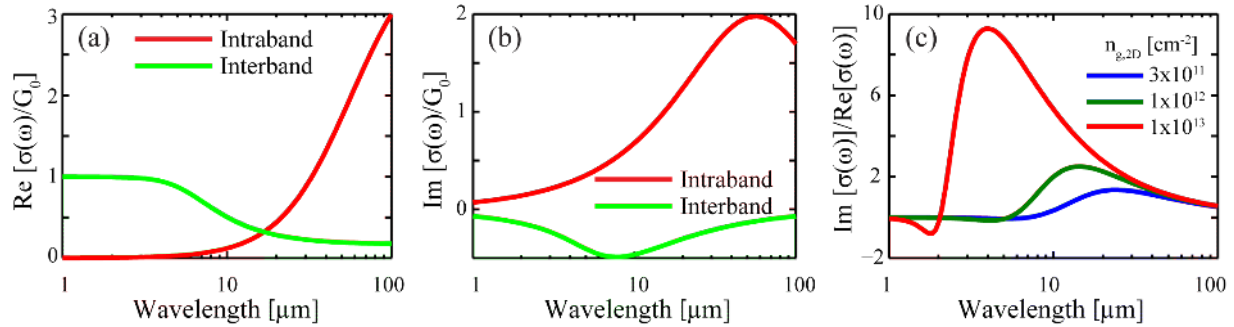


Figure 2: Relative contributions of interband and intraband transitions to real part (a) and imaginary part (b) of conductivity. Interband conductivity is dominant at visible frequencies while intraband contribution dominates above mid-infrared frequencies ($n_{g,2D} = 7 \times 10^{11} \text{ cm}^{-2}$, $T = 300 \text{ K}$, $\tau = 3 \times 10^{-14} \text{ s}$); (c) Figure of merit calculations indicating that graphene is a good plasmonic material between $2 \mu\text{m}$ – $20 \mu\text{m}$ wavelengths. The plasmonic response can be tuned to near-infrared wavelengths by increasing carrier density in graphene.

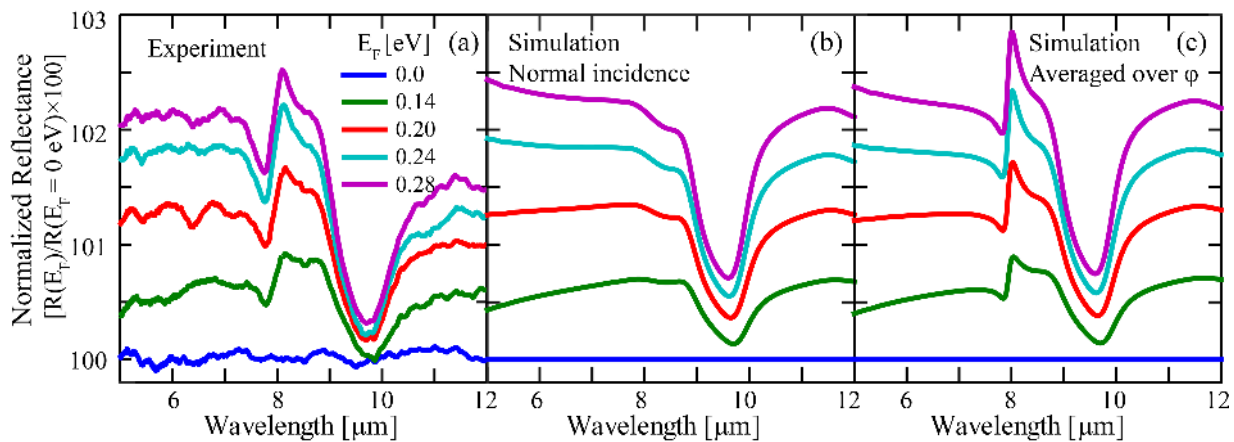


Figure 3: (a) Modulation of IR reflectivity of CVD graphene on Si/300 nm SiO_2 substrate as a function of sheet carrier density. Measurements were performed using a Fourier Transform Infrared (FTIR) Spectrometer with microscope accessory (Objective: 15X, N.A. 0.58 Reflectochromat); measurements are normalized to R_{CNP} . (b-c) FEM simulations using a surface current model for graphene (COMSOL Multiphysics) at normal incidence and averaged over a range of angle of incidence (ϕ); the experimental data was fitted with carrier scattering time (τ) as a fitting parameter in the RPA model, which yields scattering time of 10 fs.

The RPA model cannot be used directly in time domain simulations because the interband conductivity does not have a simple time domain form. Several groups report time domain simulations by either ignoring interband contribution or assuming asymptotic conditions [34–36]. These approximations are not valid at optical wavelengths or room temperature. We recently developed an accurate, multivariate time domain model for graphene using two Padé approximant terms, which accurately captures the time domain response of graphene from visible to IR wavelengths [37, 38]. This model has been already tested by combining critical-point approach [37, 38] with a surface-current enabled FDTD scheme [32, 39].

2.4 Gating techniques for control of optical properties

Electrical backgating is the most popular approach to control the charge density in the graphene sheet. In this method, a DC voltage is applied to the silicon substrate separated from the graphene sheet by a thin insulating layer. The induced carrier density can be estimated using a parallel plate capacitor model as $n_{g,2D} = C_{\text{gate}}(V_G - V_{\text{CNP}})/q$, where $C_{\text{gate}} = \epsilon_{\text{insulator}}/t_{\text{insulator}}$ is the gate capacitance, V_G is the applied gate voltage and V_{CNP} is the charge neutral point voltage and q is the charge of the electron. Thermally grown 300 nm SiO_2 , which is typically used as an insulator, gives a gate capacitance of 11.5 nF cm^{-2} . A thin insulating layer is usually preferred since it would give better capacitive control over the in-

duced charge. However, when the insulating films are thinner than 100 nm the gate leakage current increases causing the device to breakdown. The Si/SiO₂ backgating technique typically yields a highest carrier density of $\sim 7 \times 10^{12} \text{ cm}^{-2}$ taking into account device area and leakage considerations. The gate capacitive control can be slightly improved by using a high-*k* material like HfO₂ or Al₂O₃ instead of traditional SiO₂ as an insulator [40].

A simple yet effective method of achieving large carrier densities is to use an electrochemical top gate [41], wherein the gate voltage is applied to an electrolyte deposited on top of a graphene sheet (see Fig. 5a). The electrochemical gating scheme exhibits a much higher gate capacitance ($\sim \mu\text{F cm}^{-2}$) due to the formation of an extremely thin electrical double layer at the interface [42, 43]. Graphene can also be doped by exposure to chemicals such as Nitric Acid (HNO₃), Iron (III) Chloride (FeCl₃) and Gold (III) Chloride (AuCl₃), which leads to large sheets carrier density due to charge transfer reactions [44]. However, chemically doped devices are also known to degrade over time making them less robust compared to back gated devices.

3 Graphene as a platform for tunable plasmonic devices

3.1 Fundamentals

Surface plasmons enable the confinement of the incident electromagnetic energy into a subwavelength volume at the resonant wavelength. The characteristic resonant wavelength is extremely sensitive to the local dielectric environment, which can be effectively used to modulate the optical response of the resonance. The changes in optical properties of graphene described in the previous section, will perturb the plasmonic resonance in metallic nanostructures if they are fabricated close to the graphene sheet. The changes in resonance frequency due to this small dielectric perturbation can be estimated using the perturbation theory using the equation [45, 46]

$$\begin{aligned} \frac{\Delta\omega}{\omega_0} &= -\frac{\iiint_V dV \left[\left(\Delta\vec{\mu} \cdot \vec{H}_0 \right) \cdot \vec{H}_0^* + \left(\Delta\vec{\epsilon} \cdot \vec{E}_0 \right) \cdot \vec{E}_0^* \right]}{\iiint_V dV \left(\mu \cdot \vec{H}_0 \cdot \vec{H}_0^* + \epsilon \cdot \vec{E}_0 \cdot \vec{E}_0^* \right)} \\ &= -\frac{\Delta W_m + \Delta W_e}{W_m + W_e} \end{aligned} \quad (5)$$

where, ω_0 is the resonance frequency, E_0 and H_0 are unperturbed electric and magnetic fields, $\Delta\vec{\epsilon}$ is the change

in dielectric permittivity, $\Delta\vec{\mu}$ is the change magnetic permeability, W_e and W_m are the total electric and magnetic energies, respectively. The change in resonance frequency $\Delta\omega$ is large when a strong perturbation of material parameters overlaps with the electric and magnetic fields of the resonant mode leading to a large numerator contribution in Eq. 5. The integral in the numerator captures the change in the stored electromagnetic energy, whereas the denominator represents the total electromagnetic energy. Therefore, the fractional change in resonance frequency is simply proportional to fractional changes in the total electromagnetic energy. This approach provides a quantitative measure to analyze graphene-plasmonic hybrid geometries, and has been verified for dipole antennas [47] and Fano resonant metasurfaces [48] in MIR wavelengths.

3.2 Tunable MIR plasmonic devices

In recent years, many groups have attempted to combine the dynamic tunability of graphene with plasmonic resonances for IR modulator applications. The extraordinary sensitivity of plasmonic modes to the presence of graphene was first reported in split-ring resonators [49]. However, in that work the influence of carrier density and the exact nature of the interaction was not discussed [50]. Subsequent studies using bow-tie antennas addressed this issue and concluded that graphene modulates the plasmonic resonance strongly in MIR frequencies [51, 52]. The width of the plasmon resonance was found to decrease as the Fermi energy is increased. This is easily explained by considering the allowed interband transitions. At a Dirac point all interband transitions are allowed leading to higher loss and therefore wider resonance. However, as the Fermi energy is increased some of the interband transitions are blocked and hence the width of the resonance is lowered. It should be noted that despite the early promise—up to 25% peak change in transmission at a 5 μm wavelength (see Fig. 4a)—the bow-tie antennas did not show any spectral tunability. Further, the incident electromagnetic energy interacts strongly with graphene only in the narrow ($\sim 80 \text{ nm} \times 80 \text{ nm}$) neck region of the bow-tie antenna. In fact, for any dipole antenna at resonance the electromagnetic energy is confined only to the small regions around the edges of the antenna. Therefore, these geometries will not be very sensitive to changes in graphene and are not strongly tunable. An improved design for tunable resonance in MIR frequencies was proposed by Yao *et al.* where they incorporated ideas from Metal-Insulator-Metal (MIM) waveguides into the antenna geometry [53, 54]. In a clever design they stagger

two adjacent nanorod antennas so that the electric field is confined to regions between the nanorods—similar to a bonding mode in a MIM waveguide. They report improved tuning range of ~ 1100 nm at $6.5 \mu\text{m}$ wavelength (see Fig. 4b). The tunability of plasmon resonance could also be improved by using Fano resonant metallic structures, which possess overlapping dipolar and quadrupolar resonances [55, 56]. These resonant modes mutually interfere and produce much sharper spectral features, and hence show greater sensitivity to graphene. A large blue shift ($\sim 30 \text{ cm}^{-1}$) was shown using Fano resonant metasurface [48, 56] in MIR wavelengths (see Fig. 4c). The progress made by a number of research groups toward graphene-based modulation schemes is tabulated in Table 1. At mid-IR wavelengths MIM mode in plasmonic antennas and Fano resonant antennas have shown promising amplitude and spectral modulation results [56, 57]. Dynamic modulation has not received sufficiently wide attention—with only one report from Harvard University demonstrating 3 dB bandwidth of up to 20 GHz [57]. There is still significant room for further improvement of modulation speed since the intrinsic carrier transport occurs on a picosecond timescale in graphene [58].

3.3 Tunable NIR plasmonic devices

There is also tremendous interest in applying graphene to realize modulators and sensors at NIR and visible wavelengths, since it can potentially lead to devices with small footprint and high modulation speeds [59, 60]. It can be seen from Fig. 2c that large changes in conductivity in NIR frequencies occur when the carrier density in graphene is $>1 \times 10^{13} \text{ cm}^{-2}$. The conventional backgating technique is not adequate to realize such high carrier densities. Therefore, ionic liquid gating discussed earlier is typically used for experiments at NIR and visible wavelengths. Modulation of plasmonic resonance in NIR frequencies was demonstrated in nanorods [61] and dolmen structures [62]. The influence of graphene is much stronger in dolmen structures because of the higher sensitivity of Fano-type resonance. High- k dielectrics like Al_2O_3 , which provide stronger capacitive control on the charge carriers at the same gate voltage, provide yet another direction improving the maximum carrier density in graphene and thereby achieve stronger modulation [57]. In another intriguing report electrically tunable surface plasmon polaritons at visible wavelengths have been realized by exploiting the high localized electric fields at the interface of Ag nanowire and graphene to achieve the huge carrier density needed [63].

Table 1: Comparison of different approaches reported in literature demonstrating modulation of plasmonic resonance with graphene.

Geometry/Reference	Peak modulation			Electrical gate Type/Max $n_{\text{e-cv}}$ [cm^{-2}]
	Relative amplitude ($ a_{\text{on}}/a_{\text{off}} $)	λ change	Speed [GHz]	
Bowtie antennas (51)	0.25 @ $5 \mu\text{m}$	No	—	Backgate/ $7 \cdot 10^{12}$
MIM mode in plasmonic antennas (54,57)	0.1 @ $6.5 \mu\text{m}$	18% @ $6 \mu\text{m}$	0.03	Backgate/ $2 \cdot 10^{13}$
	25 @ $6 \mu\text{m}$	10% @ $6 \mu\text{m}$	20	Backgate/ 1.2×10^{13} high- k (c)
Plasmonic fano antennas (48,56)	—	2% @ $5.5 \mu\text{m}$	—	No gating (a)
	10 @ $7 \mu\text{m}$	4.6% @ $7 \mu\text{m}$	—	Backgate/ $4.8 \cdot 10^{13}$
Asymmetric split ring resonators (49)	2.5 @ $1.6 \mu\text{m}$	10% @ $1.85 \mu\text{m}$	—	No gating (a)
Gold nanorods (61)	0.3 @ $1.5 \mu\text{m}$	2% @ $1.5 \mu\text{m}$	—	Ionic top gate/ $4.8 \cdot 10^{13}$ (b)
Fano resonance in dolmen antennas (62)	0.08 @ $2.4 \mu\text{m}$	No	—	Ionic top gate/ $\sim 2.7 \cdot 10^{13}$
Graphene Ag-nanowire waveguide (63)	0.07 dB/ μm @ 659 nm	—	—	Backgate/ $9.2 \cdot 10^{13}$ (d)

Some of the data is approximated from the experimental results in the references mentioned.
(a) The change reported is obtained by comparing antennas with graphene to antennas without graphene.
(b) Gate capacitance not reported, $n_{\text{e-cv}}$ extracted from optical reflectivity measurements.
(c) Estimated by assuming a dielectric constant of 8 for Al_2O_3 . Alumina provides greater gate control and hence higher carrier density.
(d) Estimate also includes local electric field enhancement due to the nanowire in addition to gate.

3.4 Other graphene-plasmonic hybrid devices

In the last few years a number of research groups used plasmonic structures to improve the response of graphene photodetectors. The primary advantage of graphene over traditional photodetectors is its broad spectral sensitivity (due to its unique electronic band structure), fast transport properties [64] and short intrinsic lifetimes [58]. Photodetectors with speed exceeding 40 GHz [65] and intrinsic bandwidth of 260 GHz [58] have been demonstrated. One of the primary challenges for graphene based photodetectors is the small responsivity which is the result of finite optical absorption in single layer graphene. Further, the extraction of photocurrent is efficient only in the regions where there is a field gradient (typically p-n junctions). Echtermeyer et al. showed that by using plasmonic nanostructures it is possible to efficiently localize electromagnetic energy near the p-n junctions, and thereby enhance the efficiency of photodetectors by up to 20 times [66]. The plasmonic nanostructures help in improving the spectral selectivity of photodetectors and could potentially enable multicolor photodetection [67]. In addition to the direct excitation of e-h pairs in graphene, the hot electrons in plasmonic structures have also been shown to contribute to

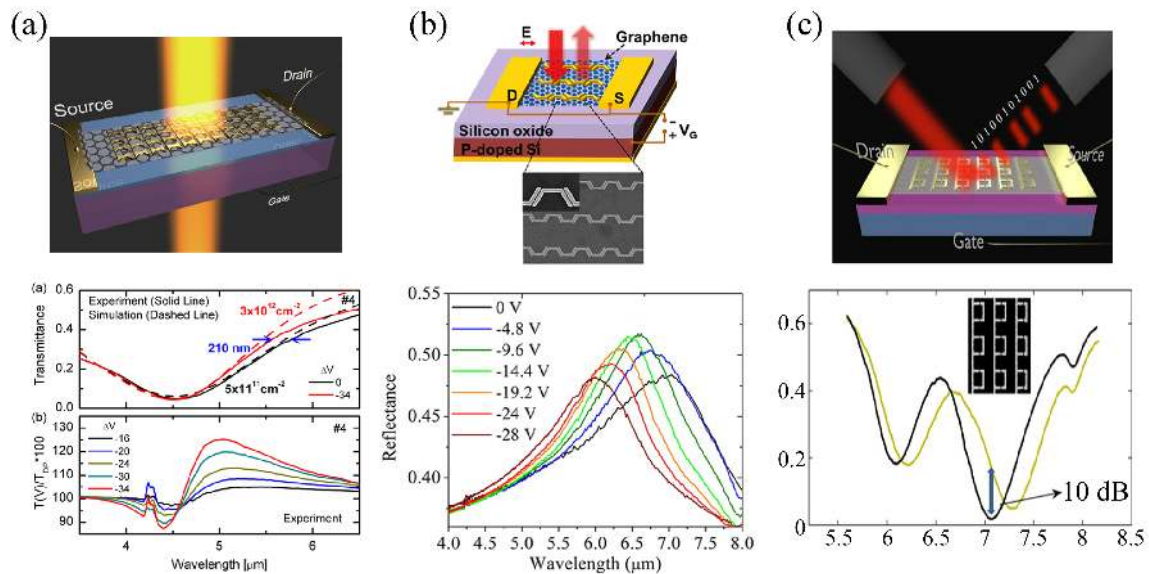


Figure 4: Dynamic modulation of plasmonic resonance at MIR wavelengths using bow-tie antennas (a), staggered nanorods mimicking bonding mode in MIM waveguides (b), and Fano resonant metasurface (c). Figures adapted with permission from references [51, 54], and [56], respectively. Copyright (2012–2014) American Chemical Society.

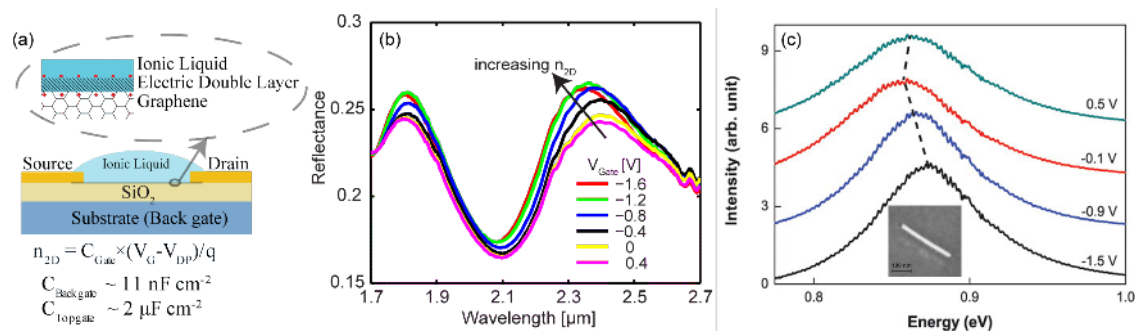


Figure 5: (a) Schematic of different gating mechanisms for graphene. Ionic top gate supports higher sheet carrier density than the conventional Si back gate due to higher capacitance; (b) modulation of Fano resonant structures at NIR wavelengths; and (c) voltage dependent scattering spectrum from a single gold nanorod covered with graphene. Figures (b) and (c) adapted with permission from references [62] and [61], respectively. Copyright (2012–2013) American Chemical Society.

photocurrent—resulting in an 800% increase in photocurrent compared to pristine graphene [68]. However, most of these experiments report improved responsivity at the cost of speed, spectral sensitivity, or device dimensions and are performed at visible wavelengths. Novel device architectures which can blend the tunability and improved responsivity of graphene-plasmonic antenna hybrid photodetector will hold significant potential for practical applications especially at IR wavelengths.

4 Conclusions and future directions

Graphene-antenna hybrid platform has shown considerable potential for the development of compact and ultrafast MIR modulators [56, 57]. There is significant scope for improvement in the NIR wavelength range where there have only been a few demonstrations [61, 62]. An important shortcoming of most of the graphene-plasmonic hybrid devices so far is the work function mismatch at the metal–graphene interface, which leads to Fermi level pinning at the interface [69]. This adversely impacts the charge transport behavior and lowers tunability of the plasmonic resonance. Mueller *et al.* report that the metal contact induced doping of graphene not only occurs un-

der the contact, but also extends 200–300 nm into the graphene sheet [70]. While it is known that metallic nanostructures cause electron doping of graphene [51], the diffusion length of carriers is presently unclear. This needs to be investigated carefully through scanning photocurrent measurements to optimize the tunability of plasmonic resonance. Another direction for improving the tunability is to increase the number of graphene layers, and thereby improve the optical conductivity [71] and strength of interaction with plasmonic resonance. Study of screening and interlayer coupling in exfoliated multilayer graphene shows that linear band structure model for graphene is valid up to four layers [72], which suggests that some of the unique properties of graphene will be preserved up to a few layers. Lastly, the experimental carrier scattering time obtained by fitting experimental IR reflectivity measurements with RPA model is only about 10 fs. Improving the uniformity of CVD-grown graphene will be very important in improving the scattering time and thereby the electro-optical response. Looking into the future, theoretical studies have shown that graphene patterned down to sizes below 10 nm can also support plasmons [73], and can potentially enable nonlinear phenomena at the single photon level [74]. Advances in the aforementioned challenges can lead to the development of exciting new technologies in addition to the NIR and MIR graphene-plasmonic antenna hybrid devices discussed in this review.

Acknowledgement: We thank Prof. Yong P. Chen, Prof. Jeorg Appenzeller, Dr. Gururaj V. Naik, Dr. Ludmila J. Prokopenko, Ting-Fung Chung, and Di Wang for helpful discussions. We also thank Clayton DeVault for help with preparation of the manuscript. The authors want to acknowledge financial support from ARO MURI Grant 56154-PH-MUR (W911NF-09-1-0539) and NSF Materials Research Science and Engineering Center (MRSEC) program DMR1120923.

References

- [1] Schuller JA, Barnard ES, Cai W, Jun YC, White JS, Brongersma ML. Plasmonics for extreme light concentration and manipulation. *Nature materials*. 2010;9(3):193-204.
- [2] Maier SA. *Plasmonics: Fundamentals and Applications*: Springer Science; 2007.
- [3] Jin EX, Xu X. Obtaining super resolution light spot using surface plasmon assisted sharp ridge nanoaperture. *Applied Physics Letters*. 2005;86(11):111106.
- [4] Challener W, Peng C, Itagi A, Karns D, Peng W, Peng Y, et al. Heat-assisted magnetic recording by a near-field transducer with efficient optical energy transfer. *Nature photonics*. 2009;3(4):220-4.
- [5] Nitzan A, Brus L. Theoretical model for enhanced photochemistry on rough surfaces. *The Journal of Chemical Physics*. 1981;75(5):2205-14.
- [6] Chen C, Osgood R. Direct observation of the local-field-enhanced surface photochemical reactions. *Physical Review Letters*. 1983;50(21):1705.
- [7] Atwater HA, Polman A. Plasmonics for improved photovoltaic devices. *Nature materials*. 2010;9(3):205-13.
- [8] Righini M, Zelenina AS, Girard C, Quidant R. Parallel and selective trapping in a patterned plasmonic landscape. *Nature Physics*. 2007;3(7):477-80.
- [9] Ndukaife JC, Mishra A, Guler U, Nnanna AGA, Wereley ST, Boltasseva A. Photothermal Heating Enabled by Plasmonic Nanostructures for Electrokinetic Manipulation and Sorting of Particles. *ACS nano*. 2014.
- [10] Anker JN, Hall WP, Lyandres O, Shah NC, Zhao J, Van Duyne RP. Biosensing with plasmonic nanosensors. *Nature materials*. 2008;7(6):442-53.
- [11] West PR, Ishii S, Naik GV, Emani NK, Shalae VM, Boltasseva A. Searching for better plasmonic materials. *Laser & Photonics Reviews*. 2010;4(6):795-808.
- [12] Naik GV, Shalae VM, Boltasseva A. Alternative plasmonic materials: beyond gold and silver. *Advanced Materials*. 2013;25(24):3264-94.
- [13] Naik GV, Liu J, Kildishev AV, Shalae VM, Boltasseva A. Demonstration of Al: ZnO as a plasmonic component for near-infrared metamaterials. *Proceedings of the National Academy of Sciences*. 2012;109(23):8834-8.
- [14] Maier SA. *Plasmonics: Fundamentals and Applications: Fundamentals and Applications*: Springer; 2007.
- [15] Driscoll T, Kim H-T, Chae B-G, Kim B-J, Lee Y-W, Jokerst NM, et al. Memory metamaterials. *Science*. 2009;325(5947):1518-21.
- [16] Chen HT, Padilla WJ, Zide JMO, Gossard AC, Taylor AJ, Averitt RD. Active terahertz metamaterial devices. *Nature*. 2006;444(7119):597-600.
- [17] Chen H-T, O'Hara JF, Azad AK, Taylor AJ, Averitt RD, Shrekenhamer DB, et al. Experimental demonstration of frequency-agile terahertz metamaterials. *Nature Photonics*. 2008;2(5):295-8.
- [18] MacDonald KF, Sámson ZL, Stockman MI, Zheludev NI. Ultrafast active plasmonics. *Nature Photonics*. 2008;3(1):55-8.
- [19] Pryce IM, Aydin K, Kelaita YA, Briggs RM, Atwater HA. Highly strained compliant optical metamaterials with large frequency tunability. *Nano Lett*. 2010;10(10):4222-7.
- [20] Xu X, Peng B, Li D, Zhang J, Wong LM, Zhang Q, et al. Flexible visible–infrared metamaterials and their applications in highly sensitive chemical and biological sensing. *Nano Lett*. 2011;11(8):3232-8.
- [21] Saito R, Dresselhaus G, Dresselhaus MS. *Physical properties of carbon nanotubes*: World Scientific; 1998.
- [22] Novoselov K, Geim A, Morozov S, Jiang D, Katsnelson M, Grigorieva I, et al. Two-dimensional gas of massless Dirac fermions in graphene. *Arxiv preprint cond-mat/0509330*. 2005.
- [23] Nair R, Blake P, Grigorenko A, Novoselov K, Booth T, Stauber T, et al. Fine structure constant defines visual transparency of graphene. *Science*. 2008;320(5881):1308-.
- [24] Khurgin J. Graphene—A rather ordinary nonlinear optical material. *Applied Physics Letters*. 2014;104(16):161116.
- [25] Mak KF, Ju L, Wang F, Heinz TF. Optical spectroscopy of graphene: from the far infrared to the ultraviolet. *Solid State*

- Comm. 2012;152(15):1341-9.
- [26] Koppens FHL, Chang DE, García de Abajo FJ. Graphene Plasmonics: A Platform for Strong Light–Matter Interactions. *Nano Letters*. 2011;11(8):3370-7.
- [27] Falkovsky L, editor. *Optical properties of graphene*. Journal of Physics: Conference Series; 2008.
- [28] Falkovsky L, Pershoguba S. Optical far-infrared properties of a graphene monolayer and multilayer. *Phys Rev B*. 2007;76(15):153410.
- [29] Li Z, Henriksen E, Jiang Z, Hao Z, Martin M, Kim P, et al. Dirac charge dynamics in graphene by infrared spectroscopy. *Nature Physics*. 2008;4(7):532-5.
- [30] Mak KF, Sfeir MY, Wu Y, Lui CH, Misewich JA, Heinz TF. Measurement of the Optical Conductivity of Graphene. *Phys Rev Lett*. 2008;101(19):196405.
- [31] Vakil A, Engheta N. Transformation optics using graphene. *Science*. 2011;332(6035):1291.
- [32] Prokopenko L, Kildishev AV, editors. *Time Domain Modeling of Tunable Graphene-Based Pulse-Shaping Device*. 30th International Review of Progress in Applied Computational Electromagnetics (ACES 2014); 2014; Jacksonville, Florida.
- [33] García de Abajo FJ. Graphene plasmonics: Challenges and opportunities. *ACS Photonics*. 2014;1(3):135-52.
- [34] Strait JH, Nene P, Chan W-M, Manolatu C, Tiwari S, Rana F, et al. Confined plasmons in graphene microstructures: Experiments and theory. *Physical Review B*. 2013;87(24):241410.
- [35] Bouzianan GD, Kantartzis NV, Antonopoulos CS, Tsiboukis TD. Optimal modeling of infinite graphene sheets via a class of generalized FDTD schemes. *Magnetics, IEEE Transactions on*. 2012;48(2):379-82.
- [36] Mock A. Padé approximant spectral fit for FDTD simulation of graphene in the near infrared. *Optical Materials Express*. 2012;2(6):771-81.
- [37] Prokopenko LJ, Emani NK, Boltasseva A, Kildishev A, editors. *Time domain modeling of tunable response of graphene*. CLEO/QELS: Fundamental Science; 2013.
- [38] Prokopenko LJ, Kildishev AV, editors. *Efficient time-domain model of the graphene dielectric function*. SPIE NanoScience and Engineering; 2013.
- [39] Prokopenko LJ, Emani NK, Boltasseva A, Kildishev A, editors. *Tunable Pulse-Shaping with Gated Graphene Nanoribbons*. CLEO/QELS; 2014.
- [40] Houssa M. *High k Gate Dielectrics*: CRC Press; 2003.
- [41] Das A, Pisana S, Chakraborty B, Piscanec S, Saha S, Waghmare U, et al. Monitoring dopants by Raman scattering in an electrochemically top-gated graphene transistor. *Nature Nanotechnology*. 2008;3(4):210-5.
- [42] Chen F, Qing Q, Xia J, Li J, Tao N. Electrochemical Gate-Controlled Charge Transport in Graphene in Ionic Liquid and Aqueous Solution. *Journal of the American Chemical Society*. 2009;131(29):9908-9.
- [43] Kim BJ, Jang H, Lee S-K, Hong BH, Ahn J-H, Cho JH. High-performance flexible graphene field effect transistors with ion gel gate dielectrics. *Nano Lett*. 2010;10(9):3464-6.
- [44] Liu H, Liu Y, Zhu D. Chemical doping of graphene. *Journal of Materials Chemistry*. 2011;21(10):3335-45.
- [45] Kong JA. *Electromagnetic Wave Theory*. USA: John Wiley and Sons; 1986.
- [46] Raman A, Fan S. Perturbation theory for plasmonic modulation and sensing. *Physical Review B*. 2011;83(20):205131.
- [47] Li Z, Yu N. Modulation of mid-infrared light using graphene-metal plasmonic antennas. *Applied Physics Letters*. 2013;102(13):131108–5.
- [48] Mousavi SH, Kholmanov I, Alici KB, Purtseladze D, Arju N, Tatar K, et al. Inductive tuning of Fano-resonant metasurfaces using plasmonic response of graphene in the mid-infrared. *Nano Lett*. 2013;13(3):1111-7.
- [49] Papasimakis N, Luo Z, Shen ZX, De Angelis F, Di Fabrizio E, Nikolaenko AE, et al. Graphene in a photonic metamaterial. *Opt Express*. 2010;18(8):8353-9.
- [50] Zou Y, Tassin P, Koschny T, Soukoulis CM. Interaction between graphene and metamaterials: split rings vs. wire pairs. *Opt Express*. 2012;20(11):12198-204.
- [51] Emani NK, Chung T-F, Ni X, Kildishev AV, Chen YP, Boltasseva A. Electrically tunable damping of plasmonic resonances with graphene. *Nano Lett*. 2012;12(10):5202-6.
- [52] Emani NK, Chung T-F, Ni X, Kildishev A, Chen YP, Boltasseva A, et al., editors. *Electrically Tunable Plasmonic Resonances with Graphene*. Quantum Electronics and Laser Science Conference; 2012: Optical Society of America.
- [53] Yao Y, Kats MA, Genevet P, Yu N, Song Y, Kong J, et al. Broad Electrical Tuning of Graphene-Loaded Plasmonic Antennas. *Nano Lett*. 2013;13(3):1257-64.
- [54] Yao Y, Kats MA, Shankar R, Song Y, Kong J, Loncar M, et al. Wide Wavelength Tuning of Optical Antennas on Graphene with Nanosecond Response Time. *Nano Lett*. 2013;14(1):214-9.
- [55] Luk'yanchuk B, Zheludev NI, Maier SA, Halas NJ, Nordlander P, Giessen H, et al. The Fano resonance in plasmonic nanostructures and metamaterials. *Nature Materials*. 2010;9(9):707-15.
- [56] Dabidian N, Kholmanov I, Khanikaev AB, Tatar K, Trendafilov S, Mousavi SH, et al. Electrical Switching of Infrared Light Using Graphene Integration with Plasmonic Fano Resonant Metasurfaces. *ACS Photonics*. 2015;2(2):216-27.
- [57] Yao Y, Shankar R, Kats M, Song Y, Kong J, Loncar M, et al. Electrically tunable metasurface perfect absorbers for ultra-thin mid-infrared optical modulators. *Nano Lett*. 2014;14(11):6526-32.
- [58] Ulrich A, Unterrainer K, Mueller T. Intrinsic response time of graphene photodetectors. *Nano Lett*. 2011;11(7):2804-8.
- [59] Liu M, Yin X, Ulin-Avila E, Geng B, Zentgraf T, Ju L, et al. A graphene-based broadband optical modulator. *Nature*. 2011;474(7349):64-7.
- [60] Bonaccorso F, Sun Z, Hasan T, Ferrari A. Graphene photonics and optoelectronics. *Nat Photonics*. 2010;4(9):611-22.
- [61] Kim J, Son H, Cho DJ, Geng B, Regan W, Shi S, et al. Electrical Control of Optical Plasmon Resonance with Graphene. *Nano Lett*. 2012;12(11):5598-602.
- [62] Emani NK, Chung T-F, Kildishev AV, Shalaev VM, Chen YP, Boltasseva A. Electrical modulation of Fano resonance in plasmonic nanostructures using graphene. *Nano Lett*. 2013;14(1):78-82.
- [63] Qian H, Ma Y, Yang Q, Chen B, Liu Y, Guo X, et al. Electrical Tuning of Surface Plasmon Polariton Propagation in Graphene–Nanowire Hybrid Structure. *ACS Nano*. 2014;8(3):2584-9.
- [64] Lin Y-M, Dimitrakopoulos C, Jenkins KA, Farmer DB, Chiu H-Y, Grill A, et al. 100-GHz transistors from wafer-scale epitaxial graphene. *Science*. 2010;327(5966):662–.
- [65] Xia F, Mueller T, Lin Y, Valdes-Garcia A, Avouris P. Ultrafast graphene photodetector. *Nature Nanotechnology*. 2009;4(12):839-43.
- [66] Echtermeyer T, Britnell L, Jasnós P, Lombardo A, Gorbachev R, Grigorenko A, et al. Strong plasmonic enhancement of photo-

- voltage in graphene. *Nature Comm.* 2011;2:458.
- [67] Liu Y, Cheng R, Liao L, Zhou H, Bai J, Liu G, et al. Plasmon resonance enhanced multicolour photodetection by graphene. *Nature Comm.* 2011;2:579.
- [68] Fang Z, Liu Z, Wang Y, Ajayan PM, Nordlander P, Halas NJ. Graphene-Antenna Sandwich Photodetector. *Nano Lett.* 2012;12(7):3808-13.
- [69] Lee E, Balasubramanian K, Weitz RT, Burghard M, Kern K. Contact and edge effects in graphene devices. *Nature Nanotechnology.* 2008;3(8):486-90.
- [70] Mueller T, Xia F, Freitag M, Tsang J, Avouris P. Role of contacts in graphene transistors: A scanning photocurrent study. *Phys Rev B.* 2009;79(24):245430.
- [71] Mak KF, Sfeir MY, Misewich JA, Heinz TF. The evolution of electronic structure in few-layer graphene revealed by optical spectroscopy. *Proc Natl Acad Sci.* 2010;107(34):14999-5004.
- [72] Sui Y, Appenzeller J. Screening and interlayer coupling in multilayer graphene field-effect transistors. *Nano Lett.* 2009;9(8):2973-7.
- [73] Thongrattanasiri S, Manjavacas A, García de Abajo FJ. Quantum finite-size effects in graphene plasmons. *ACS Nano.* 2012;6(2):1766-75.
- [74] Gullans M, Chang D, Koppens F, de Abajo FG, Lukin M. Single-photon nonlinear optics with graphene plasmons. *Phys Rev Lett.* 2013;111(24):247401.